NeuroImage: Clinical 9 (2015) 164–175

Contents lists available at ScienceDirect

NeuroImage: Clinical

journal homepage: www.elsevier.com/locate/ynicl

Detection and quantification of regional cortical gray matter damage in multiple sclerosis utilizing gradient echo MRI

Jie Wen [a], Dmitriy A. Yablonskiy [a], Jie Luo [b], Samantha Lancia [c], Charles Hildebolt [a], Anne H. Cross [c,*]

[a] Department of Radiology, Washington University, St. Louis, MO 63110, USA
[b] Research Laboratory of Electronics, Massachusetts Institute of Technology, Cambridge, MA 02139, USA
[c] Department of Neurology, Washington University, St. Louis, MO 63110, USA

ARTICLE INFO

Article history:
Received 4 May 2015
Received in revised form 3 August 2015
Accepted 4 August 2015
Available online 18 August 2015

Keywords:
Multiple sclerosis
Cortical gray matter
Quantitative
$R2^*$
Cognitive disability

ABSTRACT

Cortical gray matter (GM) damage is now widely recognized in multiple sclerosis (MS). The standard MRI does not reliably detect cortical GM lesions, although cortical volume loss can be measured. In this study, we demonstrate that the gradient echo MRI can reliably and quantitatively assess cortical GM damage in MS patients using standard clinical scanners. High resolution multi-gradient echo MRI was used for regional mapping of tissue-specific MRI signal transverse relaxation rate values ($R2^*$) in 10 each relapsing–remitting, primary-progressive and secondary-progressive MS subjects. A voxel spread function method was used to correct artifacts induced by background field gradients. $R2^*$ values from healthy controls (HCs) of varying ages were obtained to establish baseline data and calculate $\Delta R2^*$ values – age-adjusted differences between MS patients and HC. Thickness of cortical regions was also measured in all subjects. In cortical regions, $\Delta R2^*$ values of MS patients were also adjusted for changes in cortical thickness. Symbol digit modalities (SDMT) and paced auditory serial addition (PASAT) neurocognitive tests, as well as Expanded Disability Status Score, 25-foot timed walk and nine-hole peg test results were also obtained on all MS subjects. We found that $\Delta R2^*$ values were lower in multiple cortical GM and normal appearing white matter (NAWM) regions in MS compared with HC. $\Delta R2^*$ values of global cortical GM and several specific cortical regions showed significant ($p < 0.05$) correlations with SDMT and PASAT scores, and showed better correlations than volumetric measures of the same regions. Neurological tests not focused on cognition (Expanded Disability Status Score, 25-foot timed walk and nine-hole peg tests) showed no correlation with cortical GM $\Delta R2^*$ values. The technique presented here is robust and reproducible. It requires less than 10 min and can be implemented on any MRI scanner. Our results show that quantitative tissue-specific $R2^*$ values can serve as biomarkers of tissue injury due to MS in the brain, including the cerebral cortex, an area that has been difficult to evaluate using standard MRI.

1. Introduction

Multiple sclerosis (MS) is an inflammatory demyelinating disease of the brain, optic nerves and spinal cord. Involvement of gray matter in MS has long been recognized in pathology studies (Bö et al., 2007; Dawson, 1916; Klaver et al., 2013; Pirko et al., 2007; Schutzer et al., 2013), yet MS has been considered to be predominantly a white matter disease due to more readily detected focal inflammatory demyelinating pathology in white matter by histology and by MRI. Evidence exists that damage occurs frequently in NAWM (Allen et al., 2001; Moll et al., 2011; Zeis et al., 2008) and cortical gray matter (Geurts et al., 2005a; Kidd et al., 1999; Kutzelnigg et al., 2005). Damage occurring in each of these regions contributes to brain atrophy seen commonly in MS (Bermel et al., 2003; Sharma et al., 2004). Importantly, cortical lesions and cortical atrophy (which are presumed to be linked) are early findings in many RRMS patients, and correlate with disability, especially cognitive disability (Calabrese et al., 2009a; Charil et al., 2007; Zivadinov et al., 2013). Loss of cortical volume in MS does not occur in a uniform pattern, but is seen more often in specific regions such as the cingulate gyrus and insular regions (Charil et al., 2007).

Abbreviations: MS, multiple sclerosis; RRMS, relapsing–remitting multiple sclerosis; SPMS, secondary-progressive multiple sclerosis; PPMS, primary-progressive multiple sclerosis; HC, healthy control; WM, white matter; NAWM, normal appearing white matter; GM, gray matter; EDSS, expanded disability status scale; SDMT, symbol digit modalities test; PASAT, paced auditory serial addition test; 25FTW, 25-foot timed walk; 9HPT, Nine-hole peg test; GEPCI, gradient echo plural contrast imaging; MPRAGE, magnetization prepared rapid gradient echo; ROI, region of interest; WMLL, white matter lesion load; NCGMV, normalized cortical gray matter volume.

* Corresponding author at: Department of Neurology, Washington University, 660 South Euclid, Campus Box 8111, St. Louis, MO 63110, USA. Tel.: +1 314 362 3293; fax: +1 314 747 1345.
E-mail address: crossa@neuro.wustl.edu (A.H. Cross).

http://dx.doi.org/10.1016/j.nicl.2015.08.003

Unfortunately, imaging of cortical MS lesions using the MRI technique has been challenging. Although conventional T2-weighted and FLAIR MRI sequences can detect many white matter lesions, these sequences do not readily detect damage in cortical gray matter or NAWM. Many MRI techniques, such as DIR (double inversion recovery) (Calabrese et al., 2007b; Geurts et al., 2005b; Geurts et al., 2011), diffusion (Hulst et al., 2013; Llufriu et al., 2014; Vrenken et al., 2006), MT (magnetization transfer) (Chen et al., 2013; Derakhshan et al., 2014a, 2014b; Schmierer et al., 2010; Seewann et al., 2011; Yarnykh et al., 2015) and transverse relaxation rate related measurement at ultra-high field (Absinta et al., 2015; Mainero et al., 2015), have been used to improve the detection of cortical MS damage. However, for various reasons, none of them have made it into clinical practice yet.

Gradient echo plural contrast imaging (GEPCI) is a technique based on a gradient recalled echo sequence with multiple gradient echoes (Luo et al., 2012; Sati et al., 2010; Yablonskiy, 2000). GEPCI allows simultaneous generation of naturally co-registered multi-contrast images (T1-weighted or spin density images, quantitative tissue-specific $T2^*$ or $R2^*$ maps and frequency maps) from a single MRI scan. By combining basic GEPCI images, additional images can be generated, such as SWI-like images, GEPCI-SWI images, T1f images, Fluid suppressed $T2^*$ ($FST2^*$) images, and SWI-$T2^*$ images (Luo et al., 2012). Previously, using the quantitative nature of GEPCI $R2^*$ measurements, we introduced quantitative GEPCI scores of tissue damage in WM lesions (Sati et al., 2010) and demonstrated in a small cohort that quantitative GEPCI scores of cerebral WM (not including GM) correctly categorized patients into RRMS vs. SPMS vs. PPMS in 70% of cases (Luo et al., 2014). GEPCI phase images also demonstrated a potential for early MS lesion detection (Yablonskiy et al., 2012).

In this study, we use two outcomes of GEPCI approach – quantitative tissue specific $R2^*$ maps and GEPCI T1 weighted images – to study 29 MS subjects and 21 healthy controls. We applied $R2^*$ analysis to evaluate global and regional tissue integrity in MS brains, with particular focus on the cortical gray matter. The results showed significant differences between the healthy and MS cohorts. $R2^*$ results correlated with clinical and neurocognitive test scores in the MS group. Based on quantitative $R2^*$ analysis, we introduced an exhibition method, "GEPCI-barcode," to illustrate the severity of tissue damage in different brain regions in individual subjects, and to allow easy evaluation of local tissue damage based on $R2^*$ measurements.

2. Materials and methods

2.1. Subjects

Thirty MS patients with prior and clear designations as having relapsing remitting, secondary progressive or primary progressive clinical courses were invited to enroll in the study. MRI scans were collected from 10 RRMS, 10 PPMS and 10 SPMS patients. Data from one SPMS subject could not be included in final analyses because of pervasive "cloud-like" artifacts (Wen et al., 2014) caused by physiological fluctuations during the scan. The twenty one normal healthy control volunteers consisted of seven males and fourteen females, ranging in age from 21 to 74 years (age mean ± SD: 44.3 ± 14.9), were specifically chosen to represent the age range of the MS patients (Table 1). All studies were approved by the Institutional Review Board of Washington University in St Louis. All subjects provided informed consent.

2.2. Clinical testing

EDSS, a standardized neurological examination validated for use in MS, was performed by a certified examiner (AHC). Additionally, gait was assessed by 25FTW and bilateral upper extremity function was assessed by 9HPT. The PASAT, a test of auditory information processing speed and calculation ability, and SDMT, a test of visual processing speed, each validated in MS, were used to assess cognition. All testing was performed by experienced examiners on the same day as MRI, without knowledge of the imaging results.

2.3. Image acquisition

All MRI scans were collected using a 3.0 Tesla (3 T) Trio MRI scanner (Siemens, Erlangen, Germany) equipped with a 12-channel phased-array head coil. High resolution GEPCI (Luo et al., 2012; Sati et al., 2010; Yablonskiy, 2000) datasets with a voxel size of $1 \times 1 \times 3$ mm^3 were acquired using a three dimensional (3D) multi-gradient-echo

Table 1
Summary of subject demographic and clinical information.

		MS			Normative data
		RRMS	PPMS	SPMS	
Number		10	10	9	
Mean age ± SD (range)		49.4 ± 10.4 (32–60)	55.2 ± 10.2 (37–74)	59.2 ± 9.3 (45–75)	
Female/male		9/1	6/4	7/2	
SDMT mean ± SD (range)		54.6 ± 10.9 (32–68)	42.5 ± 14.5 (10–61)	44 ± 15.2 (18–63)	62.1 ± 10.7 (Strober et al., 2009)
3 s PASAT mean ± SD (range)		49.0 ± 11.6 (21–59)	40.4 ± 11 (21–56)	37.9 ± 16 (15–58)	49.7 ± 9.8 (Strober et al., 2009)
EDSS mean ± SD (range)		3.05 ± 1.7 (1–6.5)	5.1 ± 1.3 (3.5–6.5)	5.5 ± 1.1 (4–6.5)	n/a
25FTW mean ± SD (range)		5.9 ± 2.5 (3.86–12.5)	10.2 ± 9 (4.17–34.315)	13.4 ± 11 (5.5–41.08)	≤5 (Kaufman et al., 2000)
9HPT mean ± SD (range)	Dominant	23.4 ± 4.8 (16.62–30.19)	30.1 ± 9.8 (22.7–56.2)	27.5 ± 5.3 (19.9–34.69)	≤22 (Oxford Grice et al., 2003)
	Non-dominant	28.2 ± 12.8 (17.55–61.95)	31.3 ± 5.8 (24.05–41.45)	38.4 ± 19.1 (21.7–75.85)	
WMLL (ml) mean ± SD (range)		12.1 ± 13.0 (1.3–40.1)	13.1 ± 9.6 (2.3–29.2)	13.9 ± 10.0 (6.4–36.7)	
NCGMV (ml) mean ± SD (range)		757.2 ± 47.5 (703.2–835.0)	730.9 ± 55.8 (648.9–844.4)	678.3 ± 61.1 (551.2–759.1)	

SDMT = symbol digit modalities test; PASAT = paced auditory serial addition test; EDSS = expanded disability status scale; 25FTW = 25-foot timed walk; 9HPT = nine-hole peg test; WMLL = white matter lesion load; NCGMV = normalized cortical gray matter volume.

sequence with a flip angle of 30°, TR = 50 ms and total acquisition time of 6 min 30 s. For each acquisition, 11 echoes were collected with first echo time TE1 = 4 ms and echo spacing ΔTE = 4 ms. The multi-echo datasets were used for calculation of $R2^*$. Standard clinical MPRAGE (Mugler and Brookeman, 1990) images with high resolution (voxel size: 0.94 × 0.94 × 1.5 mm^3) were also collected for segmentation purposes.

2.4. Image processing

Raw k-space data were read into MATLAB (The MathWorks, Inc.) for processing. After applying Fourier transform to the k-space, data from different channels were combined for each voxel in a single data set $S(TE)$ using a strategy developed in house (Luo et al., 2012; Quirk et al., 2009):

$$S(TE) = \frac{1}{M}\sum_{m=1}^{M} \lambda_m \bar{S}(TE_1) S_m(TE_n)$$
$$\lambda_m = \frac{1}{M}\sum_{l=1}^{M} \sigma_l^2/\sigma_m^2 \quad (1)$$

where the sum is taken over all channels (m), $\bar{S}$ denotes complex conjugate of S, λ_m is the weighting parameter and σ_m is the noise amplitude (r.m.s.). We omit index corresponding to voxel position for clarity. This algorithm allows for the optimal estimation of quantitative parameters, such as magnetic resonance signal decay rate constants and also removes the initial phase incoherence between channels. $R2^*$ constants were obtained by fitting the channel-combined data on a voxel-by-voxel basis using the following theoretical model:

$$S(TE) = S_0^2 \cdot e^{-R_2^* \cdot (TE+TE_1)} \cdot e^{i\cdot\omega\cdot(TE-TE_1)} \cdot F(TE) \quad (2)$$

where ω is a local signal frequency and $F(TE)$ is the F-function describing the influence of macroscopic magnetic field inhomogeneity effects on MRI signal (Yablonskiy, 1998). Herein, we use a voxel spread function algorithm (Yablonskiy et al., 2013) for evaluation of F-function. With our choice of TR and flip angle, S_0 represents T1-weighted images. Brain segmentation and volumetric information was obtained from MPRAGE images using FreeSurfer (Martinos Center for Biomedical Imaging, MGH/HST, US). Then, ROIs were registered on GEPCI-T1w images using FSL (Analysis Group, FMRIB, Oxford, UK). Last, regional $R2^*$ median values were generated and used for further analysis, as shown in Fig. 1. Note that to minimize the partial volume effect, CSF masks were also generated based on the GEPCI T1w images using FSL (step F in Fig. 1). Volumetric data were calculated from the segmentation results by multiplying the number of voxels inside each brain region by the size of voxels. Then, normalization factors were calculated using the "SIENAX" tool in "FSL" and applied to each region to get normalized volumes. Normalized brain volume (NBV) data were also obtained from the "SIENAX" results in "FSL".

2.5. ROI creation

First (step A in Fig. 1), GEPCI-T1-weighted (S_0) images and $R2^*$ maps were generated according to Eq. (2). Both GEPCI-T1-weighted and GEPCI-$R2^*$ images were put into FSL (Jenkinson et al., 2012; Smith et al., 2004; Woolrich et al., 2009) to remove the skull. Then, MPRAGE images were put into FreeSurfer (Laboratory for Computational Neuroimaging, Martinos Center for Biomedical Imaging) to generate brain segmentations and regional masks (steps B and C in Fig. 1), which include masks for global and regional cortical gray matter, NAWM and deep gray matter (caudate, putamen, globus pallidus and thalamus).

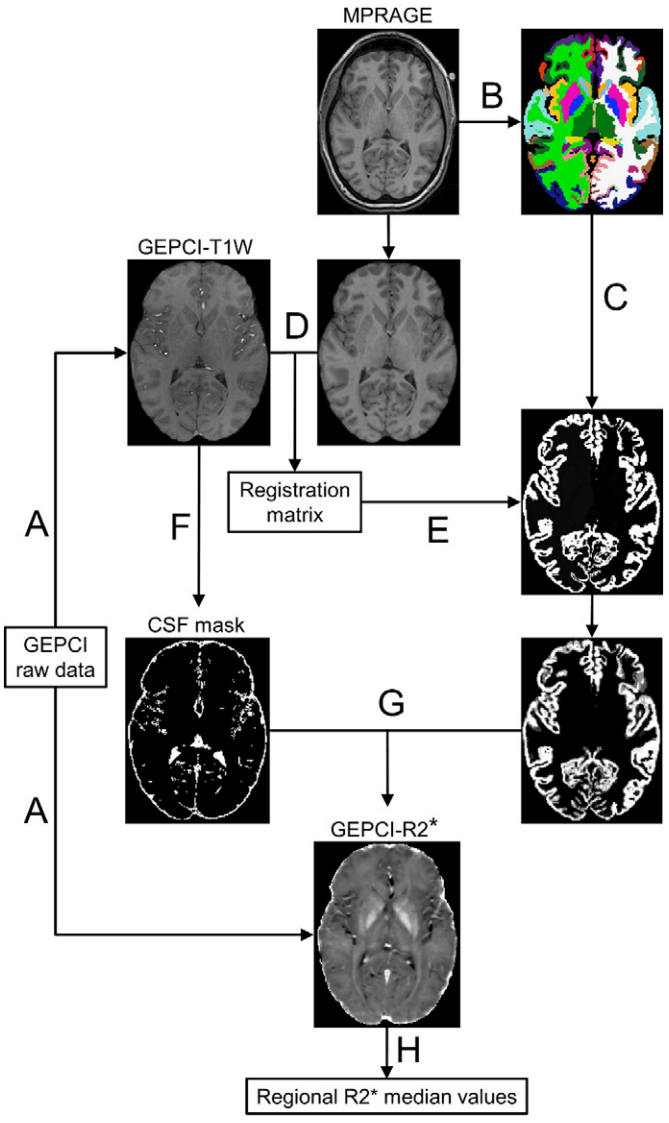

Fig. 1. Flowchart of ROI creation. A. Calculation of T1-weighted images and $R2^*$ maps from raw data, brain was extracted using BET tool in FSL; B. Freesurfer used for brain segmentation; C. generation of regional masks based on the segmentation; D. registration of MPRAGE image onto GEPCI-T1-weighted image; E. regional masks mapped onto GEPCI images; F. GEPCI-T1w images used to generate CSF mask; G & H. calculation of median values of the $R2^*$ distribution in each ROI.

At the same time, after removing skull using FSL, MPRAGE images were registered to GEPCI-T1-weighted images using FMRIB's Linear Image Registration Tool (Jenkinson et al., 2002; Jenkinson and Smith, 2001) in FSL (step D in Fig. 1) to get registration matrices. Then, the registration matrices were used to map the segmentation on GEPCI-$R2^*$ maps (step E in Fig. 1), which are naturally co-registered with GEPCI-T1-weighted images when using the GEPCI technique. To minimize the partial volume effect, CSF masks were also generated based on the GEPCI T1 weighted images using FSL (step F in Fig. 1). Note that in step B for MS subjects, we first used MPRAGE and FLAIR images to get WM lesion mask using the "lesion-TOADS" tool (Shiee et al., 2010) in MIPAV (McAuliffe et al., 2001). Then, we filled the lesion areas with averaged signal from normal tissue. These lesion-filled-MPRAGE images were used for segmentation for MS subjects. By doing this, we can minimize the topological defects caused by large lesions.

2.6. Statistical analysis

All statistical analyses were performed using MATLAB (The MathWorks, Inc.). For each ROI generated as described above, there was a distribution of $R2^*$ for which a median value was calculated. Median $R2^*$ values were used because distribution functions in each region were not symmetric. Regional $R2^*$ median values were calculated for each FreeSurfer region in each subject by applying regional and CSF masks to GEPCI $R2^*$ maps. Because age affects $R2^*$ (Siemonsen et al., 2008) and volume (Ge et al., 2002), MS subject data were corrected for age using baseline data obtained from the healthy subject cohort. Linear regression analysis of median $R2^*$ values was used to define age-dependent baseline median $R2^*$ values for each region. Based upon this formula, for each ROI for each MS subject, the age-dependent baseline median $R2^*$ value for the healthy control subjects was subtracted from the MS subject's $R2^*$ median value to obtain the age-corrected parameter, $\Delta R2^*$. The same procedure was used to create age-corrected tissue volumes, termed ΔV. In cortical GM regions, due to partial volume effect, variation in cortical thickness was also taken into account. In these regions, we adjusted $R2^*$ with respect to both age and cortical thickness using multiple linear regression to create $\Delta R2^*$. For each brain ROI, ANOVA was used to compare $\Delta R2^*$ and ΔV of the HC with MS subjects representing three clinical subtypes. Pearson's correlation was used to evaluate the correlation between $\Delta R2^*$ or ΔV values and clinical scores. Correlation coefficients (r) and p-values (p) were calculated. False discovery rate was used to correct for multiple comparisons. In all cases, a p-value <0.05 was considered as statistically significant.

2.7. GEPCI-barcode

To allow easier assimilation and comparison of the separate cortical regions, NAWM and deep gray matter regions being examined in each individual, we developed a visualization method we named "GEPCI barcode" to not only show easily distinguishable differences between healthy and MS cohorts and among different subtypes, but also to provide a potentially machine-readable representation of data relating to the regional abnormalities for each individual. For each brain ROI, the mean values ($MEAN_{HC}$) and standard deviations (STD_{HC}) of the $\Delta R2^*$ values of the healthy group were calculated. Then, z-scores were calculated for all ROIs of each MS subject using:

$$z = \frac{\Delta R2^*_{MS} - MEAN_{HC}}{STD_{HC}} \quad (3)$$

where is the $\Delta R2^*$ value calculated from distinct brain ROIs of each MS subject. All brain ROIs with z-scores between −1.96 and 1.96 were considered as normal and are shown as white squares on the barcode. Brain ROIs with z-scores less than −1.96 but greater than −2.58 were considered as regions with damage and are shown as unfilled red squares. Brain ROIs with z-scores less than −2.58 were considered as regions with severe damage, and were assigned completely red squares. Brain regions with z-score greater than 1.96 were considered as regions with high $R2^*$ values of unclear significance, and were designated unfilled blue (z-score greater than 1.96 but less than 2.58) or fully blue squares (z-score > 2.58) on the barcode.

3. Results

3.1. Cortical ROIs

$\Delta R2^*$ values of the HC and MS cohorts in the global and regional cortical GM ROIs were compared. Data from right and left sides for individual regions were combined. The MS cohort showed lower $\Delta R2^*$ values in the global cortical GM, compared with the HC cohort (Fig. 2A). When

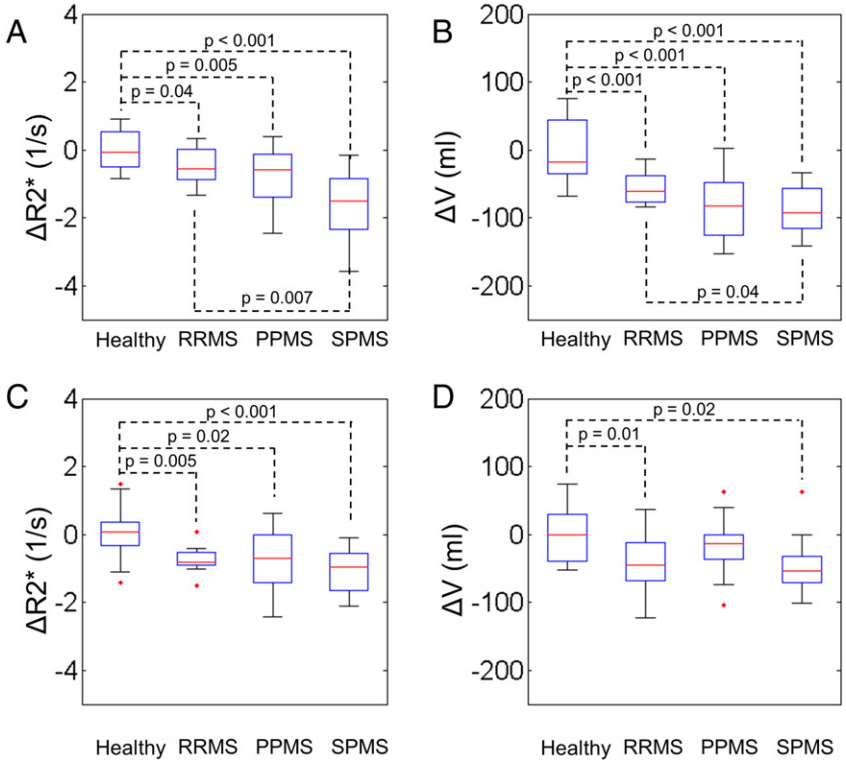

Fig. 2. $\Delta R2^*$ and normalized volumes (ΔV) of global cortical GM and NAWM for HC and MS cohorts. A. Group comparisons for $\Delta R2^*$ values in global brain cortical GM; B. group comparisons for ΔV values in global brain cortical GM; C. group comparisons for $\Delta R2^*$ values in NAWM; D. group comparisons for ΔV values in NAWM.

comparing different MS subtypes, the SPMS group showed the lowest $\Delta R2^*$ values and had the greatest number of abnormal regions, with significantly ($p < 0.05$) lower $\Delta R2^*$ values in 25 of 31 cortical regions compared with the same regions in the HC (Table A.1). MS subjects also showed significantly reduced ΔV values. Although many regions with reduced ΔV values also had reduced $\Delta R2^*$ values, in a few regions ΔV was more sensitive whereas in others $\Delta R2^*$ was more sensitive to abnormalities. Progressive MS subjects had more severe age-adjusted brain atrophy, compared to RRMS subjects. PPMS cohort had significantly decreased ΔV in 18 of 31 cortical regions, while SPMS cohort had significantly decreased ΔV in 24 of 31 cortical regions, compared to HC (Fig. 2B & Table A.1).

3.2. Non-neocortical brain ROIs

Fig. 2C reveals that the MS cohorts had lower $\Delta R2^*$ values in NAWM compared with the HCs. Significant NAWM volume loss was also found in RRMS and SPMS subjects (Fig. 2D). In the globus pallidus (Table A.1), the $\Delta R2^*$ values in the RRMS cohort were higher than the $\Delta R2^*$ values in HC. SPMS and PPMS cohorts had overall higher $\Delta R2^*$ in globus pallidus than the HC cohort but lower $\Delta R2^*$ than the RRMS cohort. No significant differences were found for $\Delta R2^*$ values in the caudate, putamen and thalamus regions between HC and any of the MS cohorts (Table A.1). ΔV values were significantly reduced in the putamen, globus pallidus, caudate and thalamus in MS subjects (Table A.1). Significant correlation was found between $\Delta R2^*$ changes in the cortex and in the thalamus ($r = 0.43$, $p = 0.002$). Only moderately significant correlation was found between $\Delta R2^*$ changes in the cortex and in the caudate ($r = 0.31$, $p = 0.03$) regions. No significant correlations were found between $\Delta R2^*$ changes in the cortex and in putamen or globus pallidus regions.

3.3. Correlations between regional $\Delta R2^*$ and ΔV values and clinical tests

SDMT and PASAT assess visual working memory speed and auditory working memory speed, respectively. $\Delta R2^*$ values calculated from the global cortical GM region correlated significantly with SDMT ($r = 0.60$, $p < 0.001$) and 3 s PASAT ($r = 0.53$, $p = 0.003$) cognitive tests (Fig. 3A & B).

$\Delta R2^*$ values in the hippocampus and many individual cortical regions also showed significant correlations with SDMT and PASAT scores as well (Table A.2). $\Delta R2^*$ values of several cortical regions correlated significantly ($r > 0.4$, $p < 0.05$) with cognitive tests (ROIs in "bold" in Table A.2). Correlations between cognitive tests and age-adjusted *whole* brain volumes (ΔNBV) were also found (Fig. 3C & D), but no significant correlations were found between normalized regional age-adjusted volumes of cortical GM and cognitive test scores (Table A.2). The multiple linear regression method was also used to test correlations between cognitive scores (SDMT and PASAT) and MRI measurements ($\Delta R2^*$ of cortical gray matter; ΔNCGMV: age-adjusted normalized cortical GM volume; WMLL: white matter lesion load). For SDMT scores, the p-values for $\Delta R2^*$, ΔNCGMV and WMLL were 0.003, 0.65 and 0.05, respectively. For PASAT scores, the p-values for $\Delta R2^*$, ΔNCGMV and WMLL were 0.005, 0.35 and 0.75, respectively. The EDSS, 25FTW and 9HPT, neurological tests that primarily assess strength, coordination, gait, and upper extremity function, showed no significant correlations with global or regional cortical GM $\Delta R2^*$ values. The 25FTW correlated inversely with ΔNBV ($r = -0.37$, $p = 0.047$) and

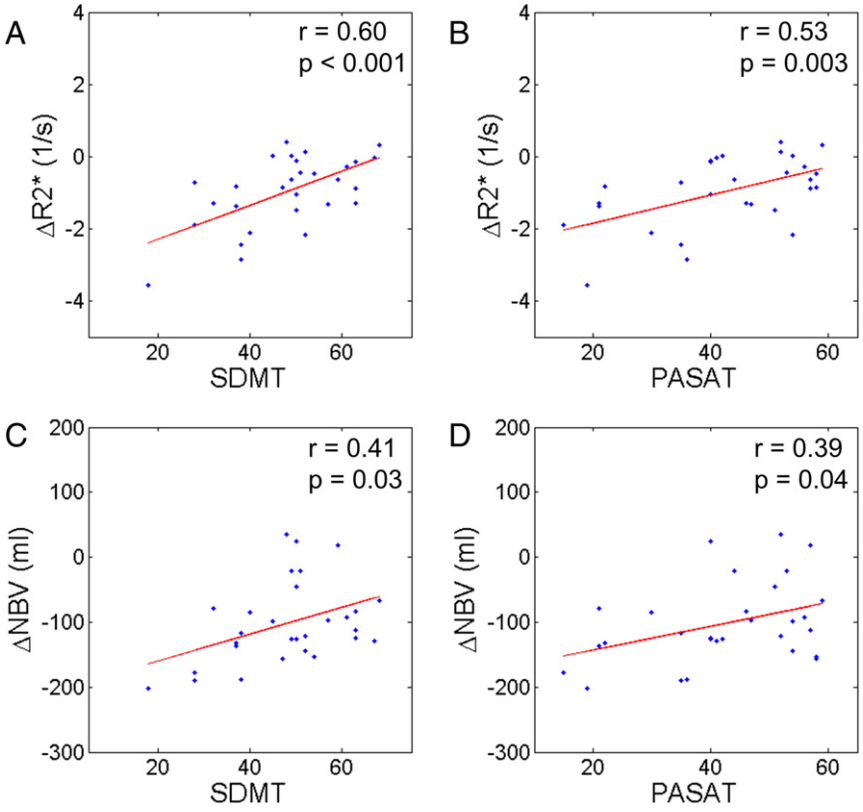

Fig. 3. Cognitive test correlations with $\Delta R2^*$ and with normalized whole brain volumes (ΔNBV). A. Correlation of $\Delta R2^*$ of global cortical GM with SDMT scores; B. correlation of $\Delta R2^*$ of global cortical GM with 3 s PASAT; C. correlation between ΔNBV and SDMT; D. correlation between ΔNBV and 3 s PASAT. Correlation coefficient (r) and p-values (p) are listed in each figure. Each point represents an individual subject. ΔNBV is the normalized whole brain volume after age correction. No significant correlations were found between regional age-adjusted cortical GM volumes and cognitive test scores (Table A.2).

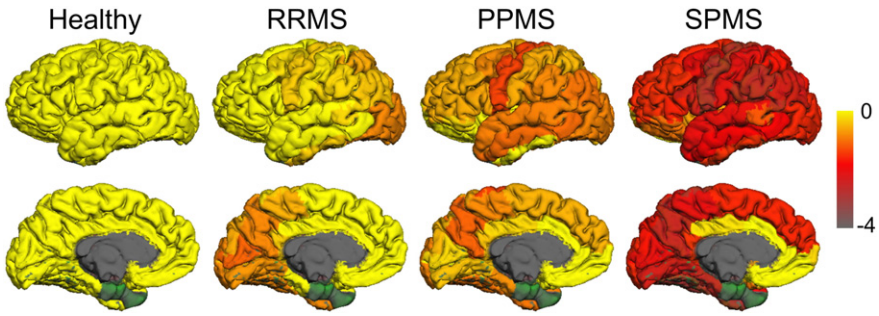

Fig. 4. Cortical z-score brain maps of $\Delta R2^*$ in healthy, RRMS, PPMS and SPMS groups. For each cortical regions in each group, averaged z-scores were calculated across all subjects.

normalized age-adjusted GM volume ($r = -0.41$, $p = 0.026$). No other correlations were found for ΔV values.

3.4. GEPCI-barcode

Averaged cortical z-score maps (from which GEPCI barcodes are derived) for four groups are shown in Fig. 4. From these z-score maps, it is apparent that most SPMS subjects have much lower GEPCI z-scores affecting almost the entire cortex.

Fig. 5 shows a summary barcode for all the subjects. As expected, most brain regions in the HC subjects were normal (white, Fig. 5). Four HC subjects showed abnormally low $\Delta R2^*$ values in a few regions (1.2% of all regions, 1.2% of cortical GM regions in all HCs). This may be explained because we selected [−1.96, 1.96] as a range to define normal $\Delta R2^*$, which contained about 95% of the total regions in HC subjects with the other 5% located outside the normal range. It is also possible that those HC subjects had real abnormalities of unknown etiology. In contrast, many brain regions of the MS subjects were abnormal (red unfilled or red filled squares for low $\Delta R2^*$; or blue unfilled or filled for high $\Delta R2^*$, Fig. 5). For cortical gray matter, the percentage of regions with abnormal tissue integrity based on GEPCI $\Delta R2^*$ values for RRMS, PPMS and SPMS subjects was 0%, 30% and 67%, respectively.

Cortical damage, inferred from the reduced $\Delta R2^*$ values, was more widespread in the SPMS cohort than the other two MS clinical subtype cohorts as illustrated with "GEPCI-barcode", with 8 of 9 SPMS subjects displaying several cortical regions of reduced $\Delta R2^*$. Interestingly, 3 of those 7 did not display reduced $\Delta R2^*$ in NAWM, supporting the finding that damage to cortical gray matter and white matter is not highly linked (Sbardella et al., 2013).

Using the GEPCI-barcode, 10% of RRMS, 30% of PPMS and 33% of SPMS subjects showed abnormally low $\Delta R2^*$ (red & black) in NAWM (Fig. 5). Regarding deep gray matter regions, in the globus pallidus, 50% of RRMS showed abnormally high $\Delta R2^*$, with fewer of the PPMS (10%) and SPMS (22%) groups with increased $\Delta R2^*$ in deep gray matter.

4. Discussion

In this study, we used tissue specific quantitative $R2^*$ values as biomarkers for tissue alterations in MS brain with particular attention to the global and regional cerebral cortex where tissue damage is poorly appreciated using standard MRI techniques. Our results conclusively support the known neuropathology of MS as a global brain disease affecting both gray and white matter. The GEPCI technique, which requires less than 7 min to acquire on standard clinical MRI scanners, detected abnormalities within regions without visible lesions, such as cortical gray matter, NAWM and deep gray matter. The measured $R2^*$ values were referenced to age-dependent HC values. The majority of white matter abnormalities were reductions in $R2^*$, which were indicative of damage based on our and others' earlier work (Cohen-Adad et al., 2011; Pitt et al., 2010; Sati et al., 2010). Further, we developed a presentation technique called "GEPCI-barcode" to display these quantitative results intuitively.

MS is a demyelinating disease of the CNS, the cause of which is yet unknown. Because it is demyelinating, it has long been considered as a white matter disease, despite the fact that myelin is also present in gray matter and initial pathology studies in the early and mid-1900s had demonstrated that both white matter and gray matter are involved (Brownell and Hughes, 1962). Reasons for the lack of attention to gray matter pathology include that focal inflammatory demyelination in gray matter provides less contrast using standard histological stains (e.g. Luxol fast blue and hematoxylin) because of the lower baseline myelin content and less prominent cellular inflammation in gray matter lesions compared with white matter MS lesions. Moreover, the pathologic changes in white matter create more conspicuous manifestations on MRI, including not only the typical hyperintensities on T2w images, but in some cases hypointensities ("black holes") on T1w images. The latter are practically never seen in gray matter. In addition to being difficult to detect on T1w and T2w images, cortical gray matter lesions have only rarely been described to enhance post-gadolinium (Popescu et al., 2011).

Yet, cortical gray matter lesions are exceedingly important in MS, and can occur very early in disease (Chard et al., 2004). Conservatively, cognitive problems affect close to half of MS patients (Rao et al., 1991). Imaging measures reflecting cortical gray matter MS pathology, such as cortical thickness and assessment of cortical lesion numbers by DIR, correlate with cognition in RRMS (Calabrese et al., 2009a; Morgen et al., 2006), and SPMS (Benedict et al., 2006; Roosendaal S.D., 2009). In contrast, measures of white matter and deep gray matter pathology (lesion volumes, black hole volumes, white matter volumes) correlate less well if at all with cognition (Roosendaal et al., 2011). Notably, cortical lesions are conspicuously sparse in patients with "benign" MS (Calabrese et al., 2009b).

Detection of cortical MS lesions using imaging in MS patients has been challenging. DIR techniques can increase cortical lesion detection (Calabrese et al., 2007b; Geurts et al., 2005b; Geurts et al., 2011), but DIR is insensitive, missing more than half of cortical MS lesions detected by histopathology (Ceccarelli et al., 2012; Seewann et al., 2012). Ultra-high field MRI detects more cortical lesions, but it is not available in most medical centers (Bluestein et al., 2012). Non-standard imaging techniques have been applied to the detection of cortical MS lesions, including magnetization transfer and diffusion tensor imaging. Cortical abnormalities detected by magnetization transfer have been reported (Chen et al., 2013; Derakhshan et al., 2014a, 2014b; Schmierer et al., 2010; Seewann et al., 2011). The findings from these studies suggested that high field and high resolution were necessary for cortical lesion detection using magnetization transfer ratio. Most of these studies were done on post-mortem brains and validated in vivo results are needed for applying this technique to clinical use. Diffusion tensor imaging is

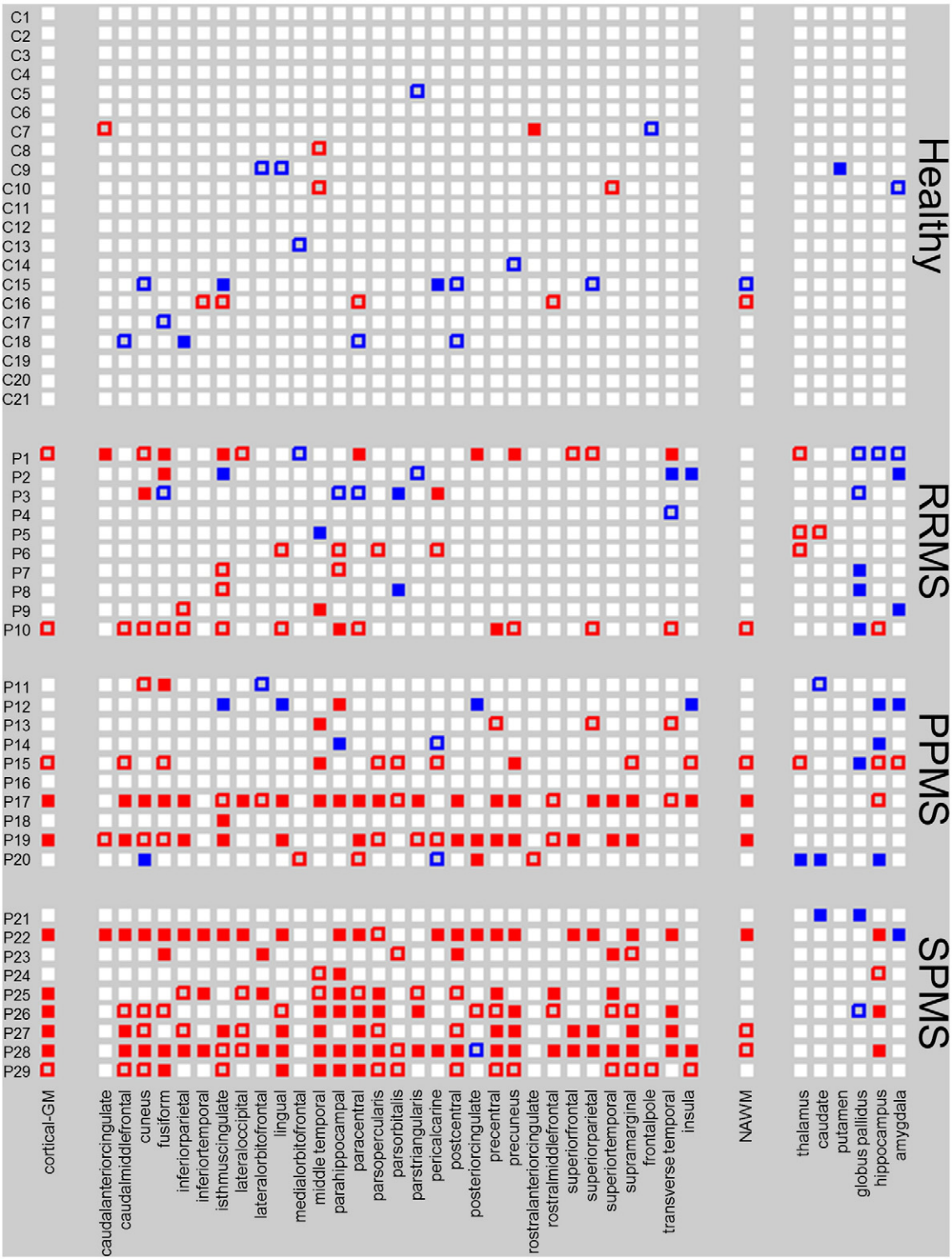

Fig. 5. GEPCI-barcodes for all brain regions studied in all subjects. $\Delta R2^*$ values were calculated for various regions (x-axis) of each HC and MS subject (y-axis). z-Score values were calculated using mean value and standard deviation calculated from age-dependent $\Delta R2^*$ values for each ROI in the whole HC cohort. White squares represent z-score values within the range −1.96 to 1.96 of the HC subjects, considered normal. Red and blue colors represent low and high $\Delta R2^*$ values, respectively. Red empty squares represent z-score values less than −1.96 but greater than −2.58. Red filled squares represent z-score values less than −2.58. Blue empty squares represent z-score values greater than 1.96 but less than 2.58. Blue filled squares represent z-score values greater than 2.58.

quantitative, and detects cortical gray matter tissue pathology (as reduced fractional anisotropy). Diffusion measures have been reported to correlate with disability, including cognitive dysfunction (Hulst et al., 2013; Vrenken et al., 2006). Application of diffusion measures in cortical gray matter, and the associations with cognitive function are still being elucidated (Llufriu et al., 2014).

GEPCI (Luo et al., 2012; Sati et al., 2010; Wen et al., 2014; Yablonskiy, 2000) is a relatively new technique, which provides high-resolution, co-registered, multi-contrast images within a single scan that can be performed in less than 7 min on standard MRI scanners (Luo et al., 2014). In this study we explored two GEPCI images — T1w and $R2^*$ maps. T1w images were used for image registration while $R2^*$ maps were used to quantify tissue "health status". Because GEPCI can provide quantitative $R2^*$ (and $T2^*$) maps, it can be used to quantitatively detect subtle tissue damage in different brain regions. Previously we used GEPCI to quantitate tissue damage in white matter lesions (Sati et al., 2010). In the present study, we report that the quantitative parameter $R2^*$ can also evaluate tissue damage in cortical gray matter and in NAWM. Our MS subject cohort showed overall substantially lower $R2^*$ values in both cortical gray matter and NAWM (Fig. 2). GEPCI data appear to provide information that is complementary to the published atrophy data (Benedict et al., 2006; Bermel et al., 2003; Calabrese et al., 2009a; Morgen et al., 2006; Zivadinov et al., 2013). Indeed our results demonstrated that not only volume but also health of the tissue as defined by $R2^*$ declined in brain regions that are also prone to suffer volume loss in MS.

Based on quantitative $R2^*$ analysis, we introduced in this paper a technique called "GEPCI-barcode" to illustrate regional GEPCI results, with the idea that this method might be applied to individually label each patient's brain tissue "health status" and follow changes in the patients' brain tissue health longitudinally. Most MS subjects in our studies had some cortical regions of $R2^*$ abnormality. Not unexpectedly, PPMS and SPMS subjects showed more widespread cortical abnormalities than RRMS subjects; this was readily apparent by viewing data using GEPCI-barcode. Abnormalities of $R2^*$ were predominantly located in the frontal, temporal, central and cingulate regions, including the caudal middle frontal, lateral orbitofrontal, paracentral, postcentral, precentral, superior temporal and isthmus of the cingulate gyrus cortical regions. Many previous studies also found that it was mainly these same regions that showed cortical atrophy in MS patients (Narayana et al., 2012a; Ramasamy et al., 2009b; van Munster et al., 2015).

Previous ex vivo studies have shown that both white matter and cortical MS lesions have shorter $R2^*$ (longer $T2^*$) due to myelin and iron loss (Yao et al., 2012; Yao et al., 2014). In accord, our MS cohort had substantially lower $R2^*$ in cortical regions compared to the healthy cohort. Moreover, GEPCI-barcode revealed more abnormal cortical regions in the SPMS than PPMS cohort in our study. This result is consistent with previous pathology studies that reported cortical demyelination in SPMS subjects to be more widespread and severe than in PPMS subjects (Howell et al., 2011; Magliozzi et al., 2007). The same study also suggested that cortical damage was distributed throughout the forebrain, especially in the deep sulci of the temporal, cingulate, insula and frontal cortex. Our results are highly consistent with this. Recently, Mainero et al. using high resolution $T2^*$ mapping obtained with high field (7 T) MRI revealed that cortical pathology has a depth dependence (Mainero et al., 2015). Their results showed that in early MS, regions with higher $T2^*$ (lower $R2^*$) were mainly located in the outer layers in the rostral anterior cingulate, parietal, precentral and postcentral regions. As disease progressed, the regions with higher $T2^*$ spread to all cortical depths and regions. Our averaged z-score map (Fig. 4) showed a similar pattern with regard to affected regions. For RRMS, the regions with lower z-scores are mainly located in the lateral occipital, parietal, cuneus, pericalcarine, precuneus, precentral and postcentral regions. For SPMS, almost all cortical regions showed low z-scores compared to other groups.

From GEPCI-barcode, we also found that one RRMS, two PPMS and four SPMS subjects showed reduced $R2^*$ in the hippocampus, a region that is crucial for episodic memory. $\Delta R2^*$ measurements in this region correlated well with SDMT and PASAT scores (Fig. 3). In our study, 6 of 7 subjects with reduced $R2^*$ in the hippocampus on GEPCI-barcode scored poorly on SDMT and PASAT testing. Again, our results are consistent with studies in which hippocampal atrophy had been found mainly in patients with severe cognitive impairment (Koenig et al., 2014; Sicotte et al., 2008). These data strongly support our interpretation of reduced $R2^*$ to indicate hippocampal damage.

Quantitative $R2^*$ analysis of global cortical gray matter showed convincing correlations with clinical cognitive tests (SDMT and PASAT). Because both SDMT and PASAT assess cognitive function in which cortical gray matter plays a critical role, this suggests that $R2^*$ can serve as a sensitive biomarker to characterize tissue functional viability. Notably, $\Delta R2^*$ values in some specific cortical regions showed strong correlations with clinical cognitive tests. The correlation between the PASAT, a measure of auditory information processing speed, and $\Delta R2^*$ values of the superior-temporal region, which is critical for auditory processing ($r = 0.62$, $p = 0.01$), supports the relevance of the GEPCI data.

We found no correlations between cortical $\Delta R2^*$ values and EDSS, 25FTW and 9HPT. These results were initially surprising, given prior papers finding correlations between GM volumes and impairment measures such as EDSS and 25FTW. However, early studies with strong correlations to EDSS often reported correlations for whole GM, including subcortical GM structures (Fisher et al., 2008; Sanfilipo et al., 2005). Others found only weak correlations between global or regional cortical thickness and physical impairment measures (Matsushita et al., 2015; Narayana et al., 2012b) or none (Datta et al., 2015; Ramasamy et al., 2009a). Many studies showing larger correlations have not accounted for age (Calabrese et al., 2007a). Our results are in keeping with the findings of Shiee et al., who found no correlation between cortical volumes and EDSS, 25FTW and 9HPT in MS patients of varying subtypes (Shiee et al., 2012). As the EDSS, 25FTW and 9HPT all measure primarily motor function and coordination, where the cerebellum and spinal cord play more important roles than the cerebral cortex, our results are not too surprising.

Importantly, our results show that regions of cortical atrophy not only suffer tissue loss but also experience tissue structural changes. Indeed, cortical damage detected by $R2^*$ measurements occurred mainly in the same regions that showed cortical atrophy in previous reports in MS patients (Narayana et al., 2012a; Ramasamy et al., 2009b). Our data confirmed volume loss in almost all of the same individual brain regions. Volume loss has been reported to correlate with cognitive impairment in RRMS (Calabrese et al., 2009a; Morgen et al., 2006). Longitudinal studies have also shown that volume loss correlates with disability (Popescu et al., 2013; Radue et al., 2015). In our cross-sectional study, we found that regional cortical GM volumetric data showed significant differences between healthy and MS cohorts, but no significant correlations of regional volumes were found with cognitive tests (Table A.2). In contrast, $R2^*$ data showed significant correlations with cognitive tests, suggesting that $R2^*$ can provide information on tissue damage in the cortex that is different and complementary to volume information.

In the deep nuclei area, especially in the globus pallidus, RRMS subjects tended to have higher $R2^*$ values compared with age-matched HC subjects (Table A.1). This is perhaps explained by excess iron accumulation in these regions, but it was curious that our progressive SPMS and PPMS cohorts demonstrated less alteration in $R2^*$ in the globus pallidus than the RRMS cohort. The reason for this is unclear, but may relate to a combination of both reduction of $R2^*$ due to tissue integrity loss and increase in $R2^*$ due to iron which serve to off-set one another in the older progressive patients to a larger degree than in the RRMS cohort.

Since cortical gray matter is relatively thin, it is important to apply methods that would reduce the influence of partial volume effects, especially signal contamination by CSF. To address this issue in our studies we used imaging with high in-plane resolution ($1\ mm \times 1\ mm$). We also applied a CSF mask to remove CSF signals that might contaminate our results and we used statistical measurements instead of a voxel-based analysis. For each region, which usually contains thousands of voxels, we generated a single parameter — median value of $R2^*$ distribution because the median value is less sensitive to outliers (that might be

related to partial volume effect). In our analysis of $R2^*$ in the cortical GM regions, we did multiple linear regression of $R2^*$ measurements with both age and cortical thickness to account for age and atrophy effects.

5. Conclusion

Our findings showed that, overall, using tissue specific $R2^*$ measurements we could detect and measure cortical abnormalities in MS patients using a standard MRI scanner, and with a very short clinically acceptable scan time. The correlations between cognitive functioning and specific gray matter $R2^*$ values provided evidence that $R2^*$ is intrinsically related to tissue-specific pathology, and $R2^*$ measurements can be used to evaluate tissue integrity. These are critical findings, as the field has great need of a quantitative method to detect cortical damage that will improve upon and complement measures of volume, which are currently the most useful measure of cortical damage (Popescu et al., 2013). Our results suggest that clinical trials, especially early phase trials using imaging as a primary endpoint, might benefit by including GEPCI measures. In future studies, we will examine larger numbers of subjects and employ methods to correct physiologically-induced artifacts (Wen et al., 2014). Our goal is to develop an easy and universally applicable quantitative method to detect CNS damage to aid in patient management and use in multi-center clinical trials.

Funding

The studies were funded by grants from the National MS Society (RG 4463A18), National Institutes of Health (CO6 RR020092) and Washington University Institute of Clinical and Translational Sciences – Brain, Behavioral and Performance Unit (TR000448). Jie Wen is a Fellow of the National MS Society USA. Anne H. Cross was funded in part by the Manny and Rosalyn Rosenthal-Dr. John L. Trotter MS Center Chair of Barnes-Jewish Hospital Foundation.

Acknowledgments

We thank Drs. Robert Naismith, Becky Jo Parks, Gregory Wu, Enrique Alvarez and Erin Longbrake for the patient referrals, and the patients and healthy subjects who participated in this study. Data management was supported by the NIH grant 5P30NS048056.

Appendix A

Table A.1
p-Values for group differences in 37 gray matter regions identified by FreeSurfer. Significant p-values ($p < 0.05$) are in bold. False discovery rate [FDR] correction for multiple comparisons was applied to all regions.

ROI	$\Delta R2^*$						Δ volume					
	HC vs. RR	HC vs. PP	HC vs. SP	RR vs. PP	RR vs. SP	PP vs. SP	HC vs. RR	HC vs. PP	HC vs. SP	RR vs. PP	RR vs. SP	PP vs. SP
Caudal anterior cingulate	0.762	0.949	0.481	0.959	0.964	0.598	0.741	0.385	0.083	0.807	0.302	0.804
Caudal middle frontal	0.341	0.101	**<0.001**	0.819	**0.039**	0.263	0.195	0.154	0.184	0.999	0.916	0.960
Cuneus	**0.041**	0.577	**<0.001**	0.819	0.287	0.255	**0.049**	**0.021**	**0.003**	0.999	0.458	0.804
Fusiform	0.136	0.101	**<0.001**	0.986	0.100	0.244	**0.009**	**0.001**	**<0.001**	0.807	0.113	0.819
Inferior parietal	0.278	0.071	**<0.001**	0.819	**0.039**	0.244	**0.049**	**0.008**	**<0.001**	0.807	0.120	0.804
Inferior temporal	0.274	0.554	**0.003**	0.819	0.135	0.244	0.084	**0.050**	0.328	0.999	0.684	0.819
Isthmus of cingulate	0.436	0.357	**0.004**	0.986	0.300	0.411	0.643	0.530	0.528	0.807	0.896	0.804
Lateral Occipital	**0.041**	0.071	**<0.001**	0.986	0.101	0.244	0.058	**0.007**	**<0.001**	0.807	0.302	0.804
Lateral orbitofrontal	0.692	0.949	**0.029**	0.819	**0.048**	0.244	0.059	**0.005**	**0.005**	0.807	0.573	0.921
Lingual	0.077	0.306	**<0.001**	0.959	0.067	0.244	**0.021**	**0.027**	**0.001**	0.999	0.304	0.804
Medial orbitofrontal	0.432	0.889	0.609	0.819	0.284	0.933	0.499	0.088	**0.018**	0.807	0.391	0.837
Middle temporal	0.804	0.086	**0.004**	0.819	0.144	0.569	**0.015**	**0.022**	**0.001**	0.999	0.638	0.804
Parahippocampal	0.738	0.215	**<0.001**	0.819	**0.039**	0.244	0.134	**0.027**	**0.012**	0.807	0.416	0.837
Paracentral	0.302	0.128	**<0.001**	0.959	0.109	0.244	0.066	**<0.001**	**0.001**	**0.012**	0.302	0.804
Pars opercularis	0.808	0.137	**<0.001**	0.819	**0.018**	0.244	**0.049**	**0.002**	**0.009**	0.807	0.702	0.837
Pars orbitalis	0.738	0.357	**0.006**	0.819	**0.039**	0.299	0.088	**0.005**	**0.017**	0.807	0.638	0.804
Pars triangularis	0.738	0.137	**<0.001**	0.819	**0.004**	0.244	**0.011**	**0.005**	**<0.001**	0.999	0.302	0.804
Pericalcarine	0.260	0.889	**0.001**	0.819	0.145	0.244	0.058	**0.021**	**0.001**	0.982	0.302	0.804
Postcentral	0.432	0.159	**<0.001**	0.819	**0.018**	0.244	**0.021**	**0.002**	**0.002**	0.807	0.573	0.837
Posterior cingulate	0.723	0.531	0.352	0.985	0.860	0.958	**0.014**	**0.022**	**<0.001**	0.999	0.197	0.804
Precentral	0.302	0.071	**<0.001**	0.819	**0.039**	0.314	**0.039**	**0.001**	**0.003**	0.800	0.521	0.819
Precuneus	0.077	0.071	**<0.001**	0.959	0.126	0.275	**0.039**	**0.006**	**0.007**	0.807	0.521	0.960
Rostral anterior cingulate	0.762	0.889	0.664	0.986	0.452	0.598	0.313	0.343	**0.009**	0.999	0.348	0.804
Rostral middle frontal	0.891	0.137	**0.003**	0.819	**0.039**	0.299	0.058	**0.040**	**0.014**	0.999	0.638	0.861
Superior frontal	0.738	0.137	**0.001**	0.819	**0.039**	0.244	0.160	**0.003**	**0.009**	0.800	0.442	0.804
Superior parietal	0.136	0.202	**<0.001**	0.986	0.101	0.244	**0.016**	**0.001**	**0.001**	0.800	0.302	0.960
Superior temporal	0.762	0.086	**<0.001**	0.819	**0.027**	0.275	**0.006**	**0.003**	**<0.001**	0.999	0.638	0.861
Supramarginal	0.339	0.137	**<0.001**	0.819	**0.039**	0.244	0.123	**0.001**	**0.001**	0.477	0.321	0.804
Frontal pole	0.891	0.666	0.232	0.819	0.284	0.583	0.162	0.245	0.908	0.999	0.416	0.804
Transverse temporal	0.762	0.720	**0.006**	0.986	0.207	0.244	0.598	0.154	0.074	0.999	0.638	0.960
Insula	0.762	0.949	0.081	0.959	0.178	0.357	**0.050**	0.347	**0.030**	0.807	0.971	0.804
Thalamus	0.329	0.949	0.307	0.819	0.691	0.583	**0.039**	**0.006**	**0.003**	0.999	0.855	0.960
Caudate	0.762	0.282	0.380	0.828	0.325	0.244	**0.006**	**<0.001**	**0.001**	0.863	0.865	0.804
Putamen	0.762	0.949	0.409	0.959	0.733	0.569	**<0.001**	**0.001**	**<0.001**	0.999	0.573	0.819
Globus pallidus	**0.041**	0.128	0.152	0.819	0.280	0.871	**0.008**	**0.006**	**<0.001**	0.999	0.397	0.804
Hippocampus	0.762	0.889	**0.008**	0.986	0.065	0.244	0.149	0.166	0.020	0.999	0.521	0.804
Amygdala	0.136	0.625	0.473	0.819	0.372	0.988	0.110	0.088	0.002	0.999	0.370	0.804

Table A.2
Correlations between cognitive test scores and $\Delta R2^*$ in 37 gray matter brain regions. Significant correlations ($r > 0.4$, $p < 0.05$) are in bold. False discovery rate [FDR] correction for multiple comparisons was applied to all regions.

ROI	$\Delta R2^*$				Δ volume			
	SDMT		PASAT (3 s)		SDMT		PASAT (3 s)	
	r	p	r	p	r	p	r	p
Caudal anterior cingulate	0.233	0.275	0.352	0.084	0.317	0.300	0.278	0.497
Caudal middle frontal	**0.557**	**0.014**	**0.480**	**0.034**	0.259	0.370	0.176	0.800
Cuneus	**0.460**	**0.028**	0.408	0.054	0.270	0.370	0.041	0.878
Fusiform	**0.551**	**0.014**	**0.501**	**0.026**	0.393	0.220	0.360	0.347
Inferior parietal	**0.514**	**0.018**	**0.517**	**0.023**	0.424	0.207	0.473	0.307
Inferior temporal	0.350	0.100	0.192	0.356	0.246	0.370	0.198	0.768
Isthmus of cingulate	0.236	0.275	0.364	0.074	0.378	0.233	0.296	0.452
Lateral occipital	0.318	0.133	0.340	0.094	0.548	0.080	0.415	0.307
Lateral orbitofrontal	**0.417**	**0.045**	0.383	0.062	0.023	0.931	0.060	0.878
Lingual	**0.533**	**0.016**	0.412	0.054	0.188	0.432	−0.041	0.878
Medial orbitofrontal	0.343	0.106	0.263	0.200	0.110	0.658	0.062	0.878
Middle temporal	0.299	0.158	0.388	0.061	0.198	0.427	0.331	0.430
Parahippocampal	**0.484**	**0.025**	0.410	0.054	0.350	0.266	0.065	0.878
Paracentral	0.200	0.356	0.264	0.200	0.332	0.299	0.147	0.808
Pars opercularis	**0.474**	**0.025**	0.405	0.054	0.203	0.424	0.158	0.808
Pars orbitalis	**0.424**	**0.043**	0.395	0.057	−0.309	0.300	−0.236	0.634
Pars triangularis	**0.474**	**0.025**	**0.525**	**0.023**	0.310	0.300	0.170	0.800
Pericalcarine	**0.473**	**0.025**	0.421	0.054	0.181	0.440	−0.044	0.878
Postcentral	**0.453**	**0.029**	**0.442**	**0.047**	0.228	0.387	0.086	0.878
Posterior cingulate	0.047	0.854	0.148	0.468	0.193	0.428	0.078	0.878
Precentral	**0.557**	**0.014**	0.396	0.057	0.292	0.338	0.203	0.768
Precuneus	**0.468**	**0.026**	**0.457**	**0.040**	0.115	0.657	0.007	0.970
Rostral anterior cingulate	0.166	0.452	0.193	0.356	0.259	0.370	0.099	0.878
Rostral middle frontal	**0.525**	**0.016**	**0.458**	**0.040**	0.069	0.783	−0.046	0.878
Superior frontal	**0.423**	**0.043**	0.406	0.054	0.155	0.518	0.029	0.907
Superior parietal	0.403	0.053	0.295	0.153	0.222	0.390	0.135	0.821
Superior temporal	**0.570**	**0.014**	**0.615**	**0.014**	0.238	0.370	0.170	0.800
Supramarginal	**0.596**	**0.014**	**0.539**	**0.023**	0.238	0.370	0.241	0.634
Frontal pole	0.376	0.075	**0.532**	**0.023**	0.050	0.843	−0.081	0.878
Transverse temporal	**0.487**	**0.025**	**0.515**	**0.023**	0.211	0.414	0.153	0.808
Insula	0.322	0.131	**0.456**	**0.040**	0.087	0.730	0.089	0.878
Thalamus	0.014	0.943	0.054	0.782	0.444	0.201	0.302	0.452
Caudate	0.148	0.496	0.092	0.651	0.010	0.960	−0.091	0.878
Putamen	−0.064	0.805	−0.170	0.412	0.405	0.220	0.300	0.452
Globus pallidus	−0.032	0.892	−0.379	0.063	0.368	0.236	0.382	0.312
Hippocampus	**0.532**	**0.016**	**0.584**	**0.016**	0.449	0.201	0.423	0.307
Amygdala	0.238	0.275	0.405	0.054	0.279	0.361	0.131	0.821

References

Absinta, M., Vuolo, L., Rao, A., Nair, G., Sati, P., Cortese, I.C., Ohayon, J., Fenton, K., Reyes-Mantilla, M.I., Maric, D., Calabresi, P.A., Butman, J.A., Pardo, C.A., Reich, D.S., 2015. Gadolinium-based MRI characterization of leptomeningeal inflammation in multiple sclerosis. Neurology. Neurology 85 (1), 18–28. http://dx.doi.org/10.1212/WNL.0000000000000158725888557.

Allen, I.V., McQuaid, S., Mirakhur, M., Nevin, G., 2001. Pathological abnormalities in the normal-appearing white matter in multiple sclerosis. Neurol. Sci. 22 (2), 141–144. http://dx.doi.org/10.1007/s10072017001211603615.

Benedict, R.H., Bruce, J.M., Dwyer, M.G., Abdelrahman, N., Hussein, S., Weinstock-Guttman, B., Garg, N., Munschauer, F., Zivadinov, R., 2006. Neocortical atrophy, third ventricular width, and cognitive dysfunction in multiple sclerosis. Arch. Neurol. 63 (9), 1301–1306. http://dx.doi.org/10.1001/archneur.63.9.130116966509.

Bermel, R.A., Sharma, J., Tjoa, C.W., Puli, S.R., Bakshi, R., 2003. A semiautomated measure of whole-brain atrophy in multiple sclerosis. J. Neurol. Sci. 208 (1–2), 57–65. http://dx.doi.org/10.1016/S0022-510X(02)00425-212639726.

Bluestein, K.T., Pitt, D., Sammet, S., Zachariah, C.R., Nagaraj, U., Knopp, M.V., Schmalbrock, P., 2012. Detecting cortical lesions in multiple sclerosis at 7 T using white matter signal attenuation. Magn. Reson. Imaging 30 (7), 907–915. http://dx.doi.org/10.1016/j.mri.2012.03.00622578928.

Bö, L., Geurts, J.J., van der Valk, P., Polman, C., Barkhof, F., 2007. Lack of correlation between cortical demyelination and white matter pathologic changes in multiple sclerosis. Arch. Neurol. 64 (1), 76–80. http://dx.doi.org/10.1001/archneur.64.1.7617210812.

Brownell, B., Hughes, J.T., 1962. The distribution of plaques in the cerebrum in multiple sclerosis. J. Neurol. Neurosurg. Psychiatry 25, 315–320. http://dx.doi.org/10.1136/jnnp.25.4.31514016083.

Calabrese, M., Agosta, F., Rinaldi, F., Mattisi, I., Grossi, P., Favaretto, A., Atzori, M., Bernardi, V., Barachino, L., Rinaldi, L., Perini, P., Gallo, P., Filippi, M., 2009a. Cortical lesions and atrophy associated with cognitive impairment in relapsing–remitting multiple sclerosis. Arch. Neurol. 66 (9), 1144–1150. http://dx.doi.org/10.1001/archneurol.2009.17419752305.

Calabrese, M., Atzori, M., Bernardi, V., Morra, A., Romualdi, C., Rinaldi, L., McAuliffe, M.J.M., Barachino, L., Perini, P., Fischl, B., Battistin, L., Gallo, P., 2007a. Cortical atrophy is relevant in multiple sclerosis at clinical onset. J. Neurol. 254 (9), 1212–1220. http://dx.doi.org/10.1007/s00415-006-0503-617361339.

Calabrese, M., De Stefano, N., Atzori, M., et al., 2007b. Detection of cortical inflammatory lesions by double inversion recovery magnetic resonance imaging in patients with multiple sclerosis. Arch. Neurol. 64 (10), 1416–1422. http://dx.doi.org/10.1001/archneur.64.10.141617923625.

Calabrese, M., Filippi, M., Rovaris, M., Bernardi, V., Atzori, M., Mattisi, I., Favaretto, A., Grossi, P., Barachino, L., Rinaldi, L., Romualdi, C., Perini, P., Gallo, P., 2009b. Evidence for relative cortical sparing in benign multiple sclerosis: a longitudinal magnetic resonance imaging study. Mult. Scler. 15 (1), 36–41. http://dx.doi.org/10.1177/1352458508096686187558 23.

Ceccarelli, A., Bakshi, R., Neema, M., 2012. MRI in multiple sclerosis: a review of the current literature. Curr. Opin. Neurol. 25 (4), 402–409. http://dx.doi.org/10.1097/WCO.0b013e328354f63f22691759.

Chard, D.T., Griffin, C.M., Rashid, W., Davies, G.R., Altmann, D.R., Kapoor, R., Barker, G.J., Thompson, A.J., Miller, D.H., 2004. Progressive grey matter atrophy in clinically early relapsing-remitting multiple sclerosis. Mult. Scler. 10 (4), 387–391. http://dx.doi.org/10.1191/1352458504ms1050oa15327034.

Charil, A., Dagher, A., Lerch, J.P., Zijdenbos, A.P., Worsley, K.J., Evans, A.C., 2007. Focal cortical atrophy in multiple sclerosis: relation to lesion load and disability. Neuroimage 34 (2), 509–517. http://dx.doi.org/10.1016/j.neuroimage.2006.10.00617112743.

Chen, J.T.-H., Easley, K., Schneider, C., Nakamura, K., Kidd, G.J., Chang, A., Staugaitis, S.M., Fox, R.J., Fisher, E., Arnold, D.L., Trapp, B.D., 2013. Clinically feasible MTR is sensitive to cortical demyelination in MS. Neurology 80 (3), 246–252. http://dx.doi.org/10.1212/WNL.0b013e31827deb9923269598.

Cohen-Adad, J., Benner, T., Greve, D., Kinkel, R.P., Radding, A., Fischl, B., Rosen, B.R., Mainero, C., 2011. In vivo evidence of disseminated subpial T2* signal changes in multiple sclerosis at 7 T: a surface-based analysis. Neuroimage 57 (1), 55–62. http://dx.doi.org/10.1016/j.neuroimage.2011.04.00921511042.

Datta, S., Staewen, T.D., Cofield, S.S., Cutter, G.R., Lublin, F.D., Wolinsky, J.S., Narayana, P.A., MRI Analysis Center at Houston, CombiRx Investigators Group, 2015. Regional gray matter atrophy in relapsing remitting multiple sclerosis: baseline analysis of multicenter data. Mult. Scler. Relat. Disord. 4 (2), 124–136. http://dx.doi.org/10.1016/j.msard.2015.01.00425787188.

Dawson, J.W., 1916. XVIII—the histology of disseminated sclerosis. Earth Environ. Sci. Transactions R. Soc. Edinb. 50 (03), 517–740. http://dx.doi.org/10.1017/S0080456800027174.

Derakhshan, M., Caramanos, Z., Narayanan, S., Arnold, D.L., Louis Collins, D., 2014a. Surface-based analysis reveals regions of reduced cortical magnetization transfer ratio in patients with multiple sclerosis: a proposed method for imaging subpial demyelination. Hum. Brain Mapp. 35 (7), 3402–3413. http://dx.doi.org/10.1002/hbm.2241024356893.

Derakhshan, M., Caramanos, Z., Narayanan, S., Arnold, D.L., Louis Collins, D., 2014b. Surface-based analysis reveals regions of reduced cortical magnetization transfer ratio in patients with multiple sclerosis: a proposed method for imaging subpial demyelination. Hum. Brain Mapp. 35 (7), 3402–3413. http://dx.doi.org/10.1002/hbm.2241024356893.

Fisher, E., Lee, J.C., Nakamura, K., Rudick, R.A., 2008. Gray matter atrophy in multiple sclerosis: a longitudinal study. Ann. Neurol. 64 (3), 255–265. http://dx.doi.org/10.1002/ana.2143618661561.

Ge, Y., Grossman, R.I., Babb, J.S., Rabin, M.L., Mannon, L.J., Kolson, D.L., 2002. Age-related total gray matter and white matter changes in normal adult brain. Part I: volumetric MR imaging analysis. A.J.N.R. Am. J. Neuroradiol. 23 (8), 1327–133312223373.

Geurts, J.J.G., Bö, L., Pouwels, P.J.W., Castelijns, J.A., Polman, C.H., Barkhof, F., 2005a. Cortical lesions in multiple sclerosis: combined postmortem MR imaging and histopathology. A.J.N.R. Am. j. neuroradiol. 26 (3), 572–57715760868.

Geurts, J.J.G., Pouwels, P.J.W., Uitdehaag, B.M.J., Polman, C.H., Barkhof, F., Castelijns, J.A., 2005b. Intracortical lesions in multiple sclerosis: improved detection with 3D double inversion-recovery MR imaging. Radiology 236 (1), 254–260. http://dx.doi.org/10.1148/radiol.236104045015987979.

Geurts, J.J.G., Roosendaal, S.D., Calabrese, M., Ciccarelli, O., Agosta, F., Chard, D.T., Gass, A., Huerga, E., Moraal, B., Pareto, D., Rocca, M.A., Wattjes, M.P., Yousry, T.A., Uitdehaag, B.M.J., Barkhof, F., MAGNIMS Study Group, 2011. Consensus recommendations for MS cortical lesion scoring using double inversion recovery MRI. Neurology 76 (5), 418–424. http://dx.doi.org/10.1212/WNL.0b013e31820a0cc421209373.

Howell, O.W., Reeves, C.A., Nicholas, R., Carassiti, D., Radotra, B., Gentleman, S.M., Serafini, B., Aloisi, F., Roncaroli, F., Magliozzi, R., Reynolds, R., 2011. Meningeal inflammation is widespread and linked to cortical pathology in multiple sclerosis. Brain 134 (9), 2755–2771. http://dx.doi.org/10.1093/brain/awr18221840891.

Hulst, H.E., Steenwijk, M.D., Versteeg, A., Pouwels, P.J., Vrenken, H., Uitdehaag, B.M., Polman, C.H., Geurts, J.J., Barkhof, F., 2013. Cognitive impairment in MS: impact of white matter integrity, gray matter volume, and lesions. Neurology 80 (11), 1025–1032. http://dx.doi.org/10.1212/WNL.0b013e31828726cc23468546.

Jenkinson, M., Bannister, P., Brady, M., Smith, S., 2002. Improved optimization for the robust and accurate linear registration and motion correction of brain images. Neuroimage 17 (2), 825–841. http://dx.doi.org/10.1006/nimg.2002.113212377157.

Jenkinson, M., Beckmann, C.F., Behrens, T.E., Woolrich, M.W., Smith, S.M., 2012. Fsl. Neuroimage 62 (2), 782–790. http://dx.doi.org/10.1016/j.neuroimage.2011.09.01521979382.

Jenkinson, M., Smith, S., 2001. A global optimisation method for robust affine registration of brain images. Med. Image Anal. 5 (2), 143–156. http://dx.doi.org/10.1016/S1361-8415(01)00036-611516708.

Kaufman, M., Moyer, D., Norton, J., 2000. The significant change for the timed 25-foot walk in the multiple sclerosis functional composite. Mult. Scler. 6 (4), 286–29010962550.

Kidd, D., Barkhof, F., McConnell, R., Algra, P.R., Allen, I.V., Revesz, T., 1999. Cortical lesions in multiple sclerosis. Brain 122 (1), 17–26. http://dx.doi.org/10.1093/brain/122.1.1710050891.

Klaver, R., De Vries, H.E., Schenk, G.J., Geurts, J.J.G., 2013. Grey matter damage in multiple sclerosis: a pathology perspective. Prion 7 (1), 66–75. http://dx.doi.org/10.4161/pri.2349923324595.

Koenig, K.A., Sakaie, K.E., Lowe, M.J., Lin, J., Stone, L., Bermel, R.A., Beall, E.B., Rao, S.M., Trapp, B.D., Phillips, M.D., 2014. Hippocampal volume is related to cognitive decline and fornicial diffusion measures in multiple sclerosis. Magn. Reson. Imaging 32 (4), 354–358. http://dx.doi.org/10.1016/j.mri.2013.12.01224512796.

Kutzelnigg, A., Lucchinetti, C.F., Stadelmann, C., Brück, W., Rauschka, H., Bergmann, M., Schmidbauer, M., Parisi, J.E., Lassmann, H., 2005. Cortical demyelination and diffuse white matter injury in multiple sclerosis. Brain 128 (11), 2705–2712. http://dx.doi.org/10.1093/brain/awh64116230320.

Llufriu, S., Martinez-Heras, E., Fortea, J., Blanco, Y., Berenguer, J., Gabilondo, I., Ibarretxe-Bilbao, N., Falcon, C., Sepulveda, M., Sola-Valls, N., Bargallo, N., Graus, F., Villoslada, P., Saiz, A., 2014. Cognitive functions in multiple sclerosis: impact of gray matter integrity. Mult. Scler. 20 (4), 424–432. http://dx.doi.org/10.1177/1352458513503722240005025.

Luo, J., Jagadeesan, B.D., Cross, A.H., Yablonskiy, D.A., 2012. Gradient echo plural contrast imaging — signal model and derived contrasts: T2*, T1, phase, SWI, T1f, FST2*and T2*-SWI. NeuroImage 60 (2), 1073–1082. http://dx.doi.org/10.1016/j.neuroimage.2012.01.10822305993.

Luo, J., Yablonskiy, D.A., Hildebolt, C.F., Lancia, S., Cross, A.H., 2014. Gradient echo magnetic resonance imaging correlates with clinical measures and allows visualization of veins within multiple sclerosis lesions. Mult. Scler. 20 (3), 349–355. http://dx.doi.org/10.1177/1352458513495935238336876.

Magliozzi, R., Howell, O., Vora, A., Serafini, B., Nicholas, R., Puopolo, M., Reynolds, R., Aloisi, F., 2007. Meningeal B-cell follicles in secondary progressive multiple sclerosis associate with early onset of disease and severe cortical pathology. Brain 130 (4), 1089–1104. http://dx.doi.org/10.1093/brain/awm03817438020.

Mainero, C., Louapre, C., Govindarajan, S.T., Giannì, C., Nielsen, A.S., Cohen-Adad, J., Sloane, J., Kinkel, R.P., 2015. A gradient in cortical pathology in multiple sclerosis by in vivo quantitative 7 T imaging. Brain 138 (4), 932–945. http://dx.doi.org/10.1093/brain/awv01125681411.

Matsushita, T., Madireddy, L., Sprenger, T., Khankhanian, P., Magon, S., Naegelin, Y., Caverzasi, E., Lindberg, R.L.P., Kappos, L., Hauser, S.L., Oksenberg, J.R., Henry, R., Pelletier, D., Baranzini, S.E., 2015. Genetic associations with brain cortical thickness in multiple sclerosis. Genes Brain Behav. 14 (2), 217–227. http://dx.doi.org/10.1111/gbb.1219025684059.

McAuliffe, M.J., Lalonde, F.M., McGarry, D., Gandler, W., Csaky, K., Trus, B.L., 2001. Medical image processing, analysis and visualization in clinical research. Proceedings of the 14th IEEE Symposium on Computer-based Medical Systems. CBMS 2001, pp. 381–386.

Moll, N.M., Rietsch, A.M., Thomas, S., Ransohoff, A.J., Lee, J.-C., Fox, R., Chang, A., Ransohoff, R.M., Fisher, E., 2011. Multiple sclerosis normal-appearing white matter: pathology–imaging correlations. Ann. Neurol. 70 (5), 764–773. http://dx.doi.org/10.1002/ana.2252122162059.

Morgen, K., Sammer, G., Courtney, S.M., Wolters, T., Melchior, H., Blecker, C.R., Oschmann, P., Kaps, M., Vaitl, D., 2006. Evidence for a direct association between cortical atrophy and cognitive impairment in relapsing–remitting MS. Neuroimage 30 (3), 891–898. http://dx.doi.org/10.1016/j.neuroimage.2005.10.03216360321.

Mugler, J.P., Brookeman, J.R., 1990. Three-dimensional magnetization-prepared rapid gradient-echo imaging (3D MP RAGE). Magn. Reson. Med. 15 (1), 152–157. http://dx.doi.org/10.1002/mrm.19101501172374495.

Narayana, P.A., Govindarajan, K.A., Goel, P., Datta, S., Lincoln, J.A., Cofield, S.S., Cutter, G.R., Lublin, F.D., Wolinsky, J.S., MRI Analysis Center at Houston; The CombiRx Investigators Group, 2012a. Regional cortical thickness in relapsing remitting multiple sclerosis: a multi-center studyNeuroimage Clin. 2, 120–131. http://dx.doi.org/10.1016/j.nicl.2012.11.00924179765.

Narayana, P.A., Govindarajan, K.A., Goel, P., Datta, S., Lincoln, J.A., Cofield, S.S., Cutter, G.R., Lublin, F.D., Wolinsky, J.S., MRI Analysis Center at Houston; The CombiRx Investigators Group, 2012b. Regional cortical thickness in relapsing remitting multiple sclerosis: a multi-center study. Neuroimage Clin. 2, 120–131. http://dx.doi.org/10.1016/j.nicl.2012.11.00924179765.

Oxford Grice, K., Vogel, K.A., Le, V., Mitchell, A., Muniz, S., Vollmer, M.A., 2003. Adult norms for a commercially available Nine Hole Peg Test for finger dexterity. Am. J. Occup. Ther. 57 (5), 570–573. http://dx.doi.org/10.5014/ajot.57.5.57014527120.

Pirko, I., Lucchinetti, C.F., Sriram, S., Bakshi, R., 2007. Gray matter involvement in multiple sclerosis. Neurology 68 (9), 634–642. http://dx.doi.org/10.1212/01.wnl.0000250267.85698.7a17325269.

Pitt, D., Boster, A., Pei, W., Wohleb, E., Jasne, A., Zachariah, C.R., Rammohan, K., Knopp, M.V., Schmalbrock, P., 2010. Imaging cortical lesions in multiple sclerosis with ultra-high-field magnetic resonance imaging. Arch. Neurol. 67 (7), 812–818. http://dx.doi.org/10.1001/archneurol.2010.14820625086.

Popescu, B.F., Bunyan, R.F., Parisi, J.E., Ransohoff, R.M., Lucchinetti, C.F., 2011. A case of multiple sclerosis presenting with inflammatory cortical demyelination. Neurology 76 (20), 1705–1710. http://dx.doi.org/10.1212/WNL.0b013e31821a44f121576686.

Popescu, V., Agosta, F., Hulst, H.E., Sluimer, I.C., Knol, D.L., Sormani, M.P., Enzinger, C., Ropele, S., Alonso, J., Sastre-Garriga, J., Rovira, A., Montalban, X., Bodini, B., Ciccarelli, O., Khaleeli, Z., Chard, D.T., Matthews, L., Palace, J., Giorgio, A., De Stefano, N., Eisele, P., Gass, A., Polman, C.H., Uitdehaag, B.M., Messina, M.J., Comi, G., Filippi, M., Barkhof, F., Vrenken, H., MAGNIMS Study Group, 2013. Brain atrophy and lesion load predict long term disability in multiple sclerosis. J. Neurol. Neurosurg. Psychiatry 84 (10), 1082–1091. http://dx.doi.org/10.1136/jnnp-2012-30409423524331.

Quirk, J.D., Sukstanskii, A.L., Bretthorst, G.L., Yablonskiy, D.A., 2009. Optimal decay rate constant estimates from phased array data utilizing joint Bayesian analysis. J. Magn. Reson. 198 (1), 49–56. http://dx.doi.org/10.1016/j.jmr.2009.01.00119181549.

Radue, E.-W., Barkhof, F., Kappos, L., Sprenger, T., Häring, D.A., de Vera, A., von Rosenstiel, P., Bright, J.R., Francis, G., Cohen, J.A., 2015. Correlation between brain volume loss and clinical and MRI outcomes in multiple sclerosis. Neurol. 84 (8), 784–793. http://dx.doi.org/10.1212/WNL.0000000000000128125632085.

Ramasamy, D.P., Benedict, R.H.B., Cox, J.L., Fritz, D., Abdelrahman, N., Hussein, S., Minagar, A., Dwyer, M.G., Zivadinov, R., 2009a. Extent of cerebellum, subcortical and cortical atrophy in patients with MS. J. Neurol. Sci. 282 (1–2), 47–54. http://dx.doi.org/10.1016/j.jns.2008.12.034.

Ramasamy, D.P., Benedict, R.H.B., Cox, J.L., Fritz, D., Abdelrahman, N., Hussein, S., Minagar, A., Dwyer, M.G., Zivadinov, R., 2009b. Extent of cerebellum, subcortical and cortical atrophy in patients with MS: a case–control study. J. Neurol. Sci. 282 (1–2), 47–54. http://dx.doi.org/10.1016/j.jns.2008.12.03419201003.

Rao, S.M., Leo, G.J., Bernardin, L., Unverzagt, F., 1991. Cognitive dysfunction in multiple sclerosis. I. Frequency, patterns, and prediction. Neurology 41 (5), 685–691.

Roosendaal, S.D., Bendfeldt, K., Vrenken, H., Polman, C.H., Borgwardt, S., Radue, E.W., Kappos, L., Pelletier, D., Hauser, S.L., Matthews, P.M., Barkhof, F., Geurts, J.J., 2011. Grey matter volume in a large cohort of MS patients: relation to MRI parameters and disability. Mult. Scler. 17 (9), 1098–1106. http://dx.doi.org/10.1177/1352458511404916215864 87.

Roosendaal, S.D., Moraal, B., Pouwels, P.J., Vrenken, H., Castelijns, J.A., Barkhof, F., Geurts, J.J., 2009. Accumulation of cortical lesions in MS: relation with cognitive impairment. Mult. Scler. 15 (6), 708–714. http://dx.doi.org/10.1177/1352458509102907194357 49.

Sanfilipo, M.P., Benedict, R.H.B., Sharma, J., Weinstock-Guttman, B., Bakshi, R., 2005. The relationship between whole brain volume and disability in multiple sclerosis: a comparison of normalized gray vs. white matter with misclassification correction. Neuroimage 26 (4), 1068–1077. http://dx.doi.org/10.1016/j.neuroimage.2005.03.00815961046.

Sati, P., Cross, A.H., Luo, J., Hildebolt, C.F., Yablonskiy, D.A., 2010. In vivo quantitative evaluation of brain tissue damage in multiple sclerosis using gradient echo plural contrast imaging technique. Neuroimage 51 (3), 1089–1097. http://dx.doi.org/10.1016/j.neuroimage.2010.03.04520338247.

Sbardella, E., Petsas, N., Tona, F., Prosperini, L., Raz, E., Pace, G., Pozzilli, C., Pantano, P., 2013. Assessing the correlation between grey and white matter damage with

motor and cognitive impairment in multiple sclerosis patients. PLOS One 8 (5), e63250. http://dx.doi.org/10.1371/journal.pone.006325023696802.
Schmierer, K., Parkes, H.G., So, P.W., An, S.F., Brandner, S., Ordidge, R.J., Yousry, T.A., Miller, D.H., 2010. High field (9.4 Tesla) magnetic resonance imaging of cortical grey matter lesions in multiple sclerosis. Brain 133 (3), 858–867. http://dx.doi.org/10.1093/brain/awp33520123726.
Schutzer, S.E., Angel, T.E., Liu, T., Schepmoes, A.A., Xie, F., Bergquist, J., Vécsei, L., Zadori, D., Camp, D.G., Holland, B.K., Smith, R.D., Coyle, P.K., 2013. Gray matter is targeted in first-attack multiple sclerosis. PLOS One 8 (9), e66117. http://dx.doi.org/10.1371/journal.pone.006611724039694.
Seewann, A., Kooi, E.J., Roosendaal, S.D., Pouwels, P.J., Wattjes, M.P., van der Valk, P., Barkhof, F., Polman, C.H., Geurts, J.J., 2012. Postmortem verification of MS cortical lesion detection with 3D DIR. Neurology 78 (5), 302–308. http://dx.doi.org/10.1212/WNL.0b013e31824528a022218278.
Seewann, A., Vrenken, H., Kooi, E.J., van der Valk, P., Knol, D.L., Polman, C.H., Pouwels, P.J., Barkhof, F., Geurts, J.J., 2011. Imaging the tip of the iceberg: visualization of cortical lesions in multiple sclerosis. Mult. Scler. 17 (10), 1202–1210. http://dx.doi.org/10.1177/1352458511406575215619 55.
Sharma, J., Sanfilipo, M.P., Benedict, R.H.B., Weinstock-Guttman, B., Munschauer, F.E., Bakshi, R., 2004. Whole-brain atrophy in multiple sclerosis measured by automated versus semiautomated MR imaging segmentation. A.J.N.R. Am. j. neuroradiol. 25 (6), 985–996 15205136.
Shiee, N., Bazin, P.L., Ozturk, A., Reich, D.S., Calabresi, P.A., Pham, D.L., 2010. A topology-preserving approach to the segmentation of brain images with multiple sclerosis lesions. Neuroimage 49 (2), 1524–1535. http://dx.doi.org/10.1016/j.neuroimage.2009.09.005 19766196.
Shiee, N., Bazin, P.L., Zackowski, K.M., Farrell, S.K., Harrison, D.M., Newsome, S.D., Ratchford, J.N., Caffo, B.S., Calabresi, P.A., Pham, D.L., Reich, D.S., 2012. Revisiting brain atrophy and its relationship to disability in multiple sclerosis. PLOS One 7 (5), e37049. http://dx.doi.org/10.1371/journal.pone.003704922615886.
Sicotte, N.L., Kern, K.C., Giesser, B.S., Arshanapalli, A., Schultz, A., Montag, M., Wang, H., Bookheimer, S.Y., 2008. Regional hippocampal atrophy in multiple sclerosis. Brain 131 (4), 1134–1141. http://dx.doi.org/10.1093/brain/awn03018375977.
Siemonsen, S., Finsterbusch, J., Matschke, J., Lorenzen, A., Ding, X.Q., Fiehler, J., 2008. Age-dependent normal values of T2* and T2′ in brain parenchyma. A.J.N.R. Am. J. Neuroradiol. 29 (5), 950–955. http://dx.doi.org/10.3174/ajnr.A095118272561.
Smith, S.M., Jenkinson, M., Woolrich, M.W., Beckmann, C.F., Behrens, T.E.J., Johansen-Berg, H., Bannister, P.R., De Luca, M., Drobnjak, I., Flitney, D.E., Niazy, R.K., Saunders, J., Vickers, J., Zhang, Y.Y., De Stefano, N., Brady, J.M., Matthews, P.M., 2004. Advances in functional and structural MR image analysis and implementation as FSL. Neuroimage 23, S208–S219. http://dx.doi.org/10.1016/j.neuroimage.2004.07.05115501092.
Strober, L., Englert, J., Munschauer, F., Weinstock-Guttman, B., Rao, S., Benedict, R.H., 2009. Sensitivity of conventional memory tests in multiple sclerosis: comparing the Rao Brief Repeatable Neuropsychological Battery and the minimal assessment of cognitive function in MS. Mult. Scler. 15 (9), 1077–1084. http://dx.doi.org/10.1177/1352458509106615195563 11.
van Munster, C.E., Jonkman, L.E., Weinstein, H.C., Uitdehaag, B.M., Geurts, J.J., 2015. Gray matter damage in multiple sclerosis: impact on clinical symptoms. Neuroscience 303, 446–461. http://dx.doi.org/10.1016/j.neuroscience.2015.07.00626164500.
Vrenken, H., Pouwels, P.J., Geurts, J.J., Knol, D.L., Polman, C.H., Barkhof, F., Castelijns, J.A., 2006. Altered diffusion tensor in multiple sclerosis normal-appearing brain tissue: cortical diffusion changes seem related to clinical deterioration. J. Magn. Reson. Imaging 23 (5), 628–636. http://dx.doi.org/10.1002/jmri.20564165659 55.
Wen, Y., Zhou, D., Liu, T., Spincemaille, P., Wang, Y., 2014. An iterative spherical mean value method for background field removal in MRI. Magn. Reson. Med. 72 (4), 1065–1071. http://dx.doi.org/10.1002/mrm.24998.
Woolrich, M.W., Jbabdi, S., Patenaude, B., Chappell, M., Makni, S., Behrens, T., Beckmann, C., Jenkinson, M., Smith, S.M., 2009. Bayesian analysis of neuroimaging data in FSL. Neuroimage 45 (1 Suppl), S173–S186. http://dx.doi.org/10.1016/j.neuroimage.2008.10.05519059349.
Yablonskiy, D.A., 1998. Quantitation of intrinsic magnetic susceptibility-related effects in a tissue matrix. Phantom study. Magn. Reson. Med. 39 (3), 417–428 9498598.
Yablonskiy, D.A., 2000. Gradient echo plural contrast imaging (GEPCI) — new fast magnetic resonance imaging technique for simultaneous acquisition of T2, T1 (or spin density) and T2*-weighted images. Radiology 217, 204.
Yablonskiy, D.A., Luo, J., Sukstanskii, A.L., Iyer, A., Cross, A.H., 2012. Biophysical mechanisms of MRI signal frequency contrast in multiple sclerosis. Proc. Natl. Acad. Sci. U. S. A. 109 (35), 14212–14217. http://dx.doi.org/10.1073/pnas.120603710922891307.
Yablonskiy, D.A., Sukstanskii, A.L., Luo, J., Wang, X., 2013. Voxel spread function method for correction of magnetic field inhomogeneity effects in quantitative gradient-echo-based MRI. Magn. Reson. Med. 70 (5), 1283–1292. http://dx.doi.org/10.1002/mrm.2458523233445.
Yao, B., Bagnato, F., Matsuura, E., Merkle, H., van Gelderen, P., Cantor, F.K., Duyn, J.H., 2012. Chronic multiple sclerosis lesions: characterization with high-field-strength MR imaging. Radiology 262 (1), 206–215. http://dx.doi.org/10.1148/radiol.1111060122084205.
Yao, B., Hametner, S., van Gelderen, P., Merkle, H., Chen, C., Lassmann, H., Duyn, J.H., Bagnato, F., 2014. 7 Tesla magnetic resonance imaging to detect cortical pathology in multiple sclerosis. PLOS One 9 (10), e108863. http://dx.doi.org/10.1371/journal.pone.010886325303286.
Yarnykh, V.L., Bowen, J.D., Samsonov, A., Repovic, P., Mayadev, A., Qian, P., Gangadharan, B., Keogh, B.P., Maravilla, K.R., Jung Henson, L.K., 2015. Fast whole-brain three-dimensional macromolecular proton fraction mapping in multiple sclerosis. Radiology 274 (1), 210–220. http://dx.doi.org/10.1148/radiol.1414052825208343.
Zeis, T., Graumann, U., Reynolds, R., Schaeren-Wiemers, N., 2008. Normal-appearing white matter in multiple sclerosis is in a subtle balance between inflammation and neuroprotection. Brain 131 (1), 288–303. http://dx.doi.org/10.1093/brain/awm29118056737.
Zivadinov, R., Tekwe, C., Bergsland, N., Dolezal, O., Havrdova, E., Krasensky, J., Dwyer, M.G., Seidl, Z., Ramasamy, D.P., Vaneckova, M., Horakova, D., 2013. Bimonthly evolution of cortical atrophy in early relapsing–remitting multiple sclerosis over 2 years: a longitudinal study. Mult. Scler. Int. 2013, 231345. http://dx.doi.org/10.1155/2013/231345 23134523365753.